Fecal Microbial Profiles and Short-Chain Fatty Acid/Bile Acid Metabolomics in Patients With Age-Related Macular Degeneration: A Pilot Study

Zaid Parekh,[1] Jason Xiao,[1] Amir Mani,[2] Quadis Evans,[2] Christopher Phung,[1] Hugo A. Barba,[2] Bingqing Xie,[3] Ashley M. Sidebottom,[4] Anitha Sundararajan,[4] Huaiying Lin,[4] Ramanujam Ramaswamy,[4] David Dao,[2] Reem Gonnah,[2] Madeleine Yehia,[2] Seenu M. Hariprasad,[2] Mark D'Souza,[4] Dinanath Sulakhe,[4] Eugene B. Chang,[3,4] and Dimitra Skondra[2]

[1]Pritzker School of Medicine, The University of Chicago, Chicago, Illinois, United States
[2]Department of Ophthalmology and Visual Science, The University of Chicago, Chicago, Illinois, United States
[3]Department of Medicine, The University of Chicago, Chicago, Illinois, United States
[4]Duchossois Family Institute, The University of Chicago, Chicago, Illinois, United States

Correspondence: Dimitra Skondra, Department of Ophthalmology and Visual Science, The University of Chicago, 5841 Maryland Avenue MC2114, S-426, Chicago, IL 60637-1234, USA; dskondra@bsd.uchicago.edu.

ZP and JX are joint first authors.

Received: April 11, 2024
Accepted: February 25, 2025
Published: April 9, 2025

Citation: Parekh Z, Xiao J, Mani A, et al. Fecal microbial profiles and short-chain fatty acid/bile acid metabolomics in patients with age-related macular degeneration: A pilot study. *Invest Ophthalmol Vis Sci.* 2025;66(4):21. https://doi.org/10.1167/iovs.66.4.21

Purpose. Age-related macular degeneration (AMD) is a multifactorial disease, and studies have implicated the role of gut microbiota in its pathogenesis. However, characterization of microbiome dysbiosis and associated microbial-derived metabolomic profiles across AMD stages remains unknown. In this pilot study, we explored how gut microbiome composition and gut-derived metabolites differ in AMD.

Methods. Our pilot study analyzed fasted stool samples that were collected from 22 patients at a tertiary academic center. Subjects were classified as control, intermediate AMD, or advanced AMD based on clinical presentation. 16S rRNA amplicon sequencing and standard chromatography–mass spectrometry methods were used to identify bacterial taxonomy composition and abundance of short-chain fatty acids (SCFAs) and bile acids (BAs), respectively. Genetic testing was used to investigate the frequency of 14 high-risk single nucleotide polymorphisms (SNPs) associated with AMD in the AMD cohort.

Results. Forty-three differentially abundant genera were present among the control, intermediate, and advanced groups. Taxa with known roles in immunologic pathways, such as Desulfovibrionales ($q = 0.10$) and *Terrisporobacter* ($q = 1.16\text{e-}03$), were in greater abundance in advanced AMD patients compared to intermediate. Advanced AMD patients had decreased abundance of 12 SCFAs, including acetate ($P = 0.002$), butyrate ($P = 0.04$), and propionate ($P = 0.01$), along with 12 BAs, including taurocholic acid ($P = 0.02$) and tauroursodeoxycholic acid ($P = 0.04$). Frequencies of high-risk SNPs were not significantly different between the intermediate and advanced AMD groups.

Conclusions. This pilot study identifies distinct gut microbiome compositions and metabolomic profiles associated with AMD and its stages, providing preliminary evidence of a potential link between gut microbiota and AMD pathogenesis. To validate these findings and elucidate the underlying mechanisms, future research with larger cohorts and more comprehensive sampling is strongly recommended.

Keywords: macular degeneration, microbiome, metabolism, short chain fatty acids, bile acids

Age-related macular degeneration (AMD) is a progressive multifactorial disease that affects the macula, the central region of the retina, and it is the third leading cause of blindness in adults over 50 years old worldwide.[1–3] Depending on its presentation, AMD is generally classified in three stages. The early stage involves the buildup of extracellular substances beneath the retinal layer, termed drusen, which compromise the functionality of the retinal pigment epithelium (RPE) and disturb metabolic exchange between the RPE and choroid. The intermediate stage presents as larger drusen, and the advanced stage manifests as either geographic atrophy (GA) or choroidal neovascularization (CNV) that can cause hemorrhage and fluid leakage. All stages of AMD have been associated with chronic low-grade inflammation and oxidative stress, which over time contribute to retinal damage and photoreceptor death.[4,5]

Currently, no curative treatment exists for AMD, and the therapies that are available for advanced stages only are

invasive, expensive, high risk, and limited in their long-term effectiveness. Therefore, the identification of new preventive strategies and therapeutic approaches for AMD is of great clinical and public health importance. Several modifiable environmental and lifestyle factors, such as smoking, obesity, and a high-fat diet (HFD), have been implicated in AMD pathogenesis and progression; however, the underlying mechanisms of such factors remain poorly understood.[6–9] For these reasons, a better understanding of the mechanisms connecting environmental risk factors and AMD development has the potential to unveil new therapeutic targets for safe and non-invasive treatment, potentially leading to significant public health benefits and cost savings.

Recent evidence has suggested that the gut microbiome may serve as the missing link connecting diet and lifestyle with AMD. The complex community of microorganisms that inhabit the gastrointestinal tract has been shown to play a critical role in the modulation of systemic and local inflammation, immunity, and metabolism.[10–14] Moreover, the disruption of its normal composition and function (dysbiosis) has been associated with several chronic diseases, including inflammatory bowel disease, type 2 diabetes, and neurodegenerative disorders such as Alzheimer's disease.[15] Emerging evidence using in vivo mouse models has specifically demonstrated the key role of the gut–retina axis and diet-induced changes to the gut microbiome in AMD pathogenesis.[11,13,16] The gut microbiota has demonstrated the ability to modulate the expression and pathways of multiple genes in the retina and choroid/RPE and have known key roles in AMD pathogenesis such as AMP-activated protein kinase (AMPK), mitogen-activated protein kinase (MAPK), mitochondrial biogenesis, oxidative stress, autophagy, cell adhesion/chemotaxis, and choroidal neovascularization, which is the hallmark sign of advanced wet AMD.[12] Finally, recent case–control studies have shown dysbiosis in the gut microbiome of neovascular AMD patients compared to healthy controls, with the former having higher abundance of pathogenic bacteria genera within the Firmicutes phylum that have been shown to contribute to disruptions in metabolic and immune function.[10,14,17] However, little is known about how these findings differ between stages of AMD in patients or how the abundance of gut-derived metabolites such as short-chain fatty acids (SCFAs) and bile acids (BAs), which are powerful signaling molecules implicated in various retinal diseases, may be affected.[18] In this pilot study, we investigated the gut microbiota composition and fecal levels of microbial-derived SCFA and BA metabolites in AMD patients at different stages compared to age-matched controls without AMD.

Methods

Recruitment

Participants were recruited from The University of Chicago Eye Center. This study was conducted in accordance with the tenets of the Declaration of Helsinki and approved by the Institutional Review Board of The University of Chicago Medicine. All eligible patients underwent standard retinal evaluation and, after receiving oral and written information, gave written informed consent to participate in the study. Standard eligibility criteria required participants be over the age of 18 years and meet the requirement for written consent. Participants were excluded if they presented with other vitreoretinal diseases or a current known infection; had a history of antibiotic use less than 3 months prior to their sample collection visit; were currently undergoing radiation therapy, stem cell transplantation, or cytotoxic cancer treatments or had a history of such treatments within 1 year prior to sample collection[19]; had a history of solid organ transplantation; or had active uncontrolled or relapsing gastroenteric diseases or recent gastroenteric surgery that in the judgement of the principal investigator would affect the gut microbiome.[20,21] Participants recruited to the disease cohort had clinically confirmed diagnoses of AMD. AMD status in each eye was classified using a five-step severity scale, and patients were further categorized as either advanced or intermediate based on clinical guidelines from the American Academy of Ophthalmology and the Age-Related Eye Disease Study (AREDS)/AREDS2, which require evaluation of drusen and GA within 2 disc diameters of the center of the macula.[22–24] GA was indicated if the lesion had a diameter $\geq$ 433 µm (AREDS circle I-2) and exhibited at least two of the following features: absence of RPE pigment, circular shape, or sharp margins. Intermediate AMD was characterized by the presence of extensive intermediate drusen, at least 1 large drusen ($\geq$125 µm in diameter), or GA not involving the foveal center (500 µm centrally). Advanced AMD was characterized by GA involving the foveal center or having a total area $\geq$ 1.27 mm^2 (equivalent to a 1500-µm circle) or any features of neovascular AMD/CNV and any of its potential sequelae. The severity level of subjects was classified based on the worse eye. Control subjects were selected to represent an age- and sex-matched group with no diagnoses of AMD, retinopathy or maculopathy, glaucoma, or any systemic, metabolic, autoimmune, gastrointestinal, hepatobiliary, or cardiovascular diseases that in the judgment of the principal investigator and based on current literature would affect the gut microbiome.[25]

Sample Collection

Following recruitment and consent, all participants were given a stool sample collection kit and instructed to provide fasted stool samples at their next scheduled visit or at any time following the formal signing of the informed consent form. All patients produced samples on the morning of the collection visit and immediately sealed them in our collection kits along with cold packs and an Oxoid AnaeroGen anaerobe gas generator sachet (Thermo Fisher Scientific, Waltham, MA, USA) to preserve metabolite concentrations. The coded samples without protected health information were immediately aliquoted inside the anaerobic chamber upon retrieval, frozen, and transferred to The University of Chicago Duchossois Family Institute (DFI) Microbiome Center, where they were stored at −80°C until the initiation of processing for metagenomic and metabolomic testing. Buccal surface samples were also collected from AMD subjects for use in the commercial Macula Risk genetic test (Arctic Medical Laboratories, Grand Rapids, MI, USA), which assesses commonly occurring genetic variations associated with the progression of AMD.[26,27] Subject participation concluded when all samples and data had been collected.

Sample Processing

DNA Extraction From Fecal Material. Fecal samples were aliquoted within 24 hours into 1.5-mL freezer vials and stored at −80°C. DNA was extracted using

the QIAamp PowerFecal Pro DNA kit (QIAGEN, Hilden, Germany). Prior to extraction, samples were subjected to mechanical disruption using a bead-beating method. Briefly, samples were suspended in a QIAGEN bead tube along with lysis buffer. All samples were homogenized on the QIAGEN TissueLyser II. Samples were then centrifuged, and supernatant was resuspended in CD2, which effectively removes inhibitors by precipitating non-DNA organic and inorganic materials, including polysaccharides, cell debris, and proteins. DNA was purified routinely using a silica spin column filter membrane. By adding solution CD3, a high-concentration salt solution, DNA selectively binds to the membrane which is recovered using elution buffer. DNA is then quantified using Qubit.

Metabolite Extraction From Fecal Material. Metabolites were extracted with the addition of extraction solvent (80% methanol spiked with internal standards and stored at −80°C) to pre-weighed fecal/cecal samples at a ratio of 100 mg of material per milliliter of extraction solvent in Fisherbrand Bead Mill tubes (15-340-154; Thermo Fisher Scientific). Samples were homogenized at 4°C on a Bead Mill 24 homogenizer (15-340-163; Thermo Fisher Scientific), set at 1.6 m/s with six 30-second cycles, 5 seconds off per cycle. Samples were then centrifuged at −10°C and 20,000*g* for 15 minutes, and the supernatant was used for subsequent metabolomics analysis.

Microbiome Taxonomic Analysis

16s rRNA Amplicon Sequencing. The V4–V5 region of the 16S rRNA gene was amplified using universal bacterial primers: 563F (5′-nnnnnnnn-NNNNNNNNNNNN-AYTGGGYDTAAA-GNG-3′) and 926R (5′-nnnnnnnn-NNNNNNNNNNNN-CCGTCAATTYHT-TTRAGT-3′), where N represents the barcodes, and n is an additional nucleotide added to offset primer sequencing. The approximately ~412-bp amplicons were then purified using a spin column–based method (MinElute; QIAGEN), quantified, and pooled at equimolar concentrations. Illumina sequencing-compatible combinatorial dual index (CDI) adapters were ligated onto the pools using the QIAseq 1-Step Amplicon Library Kit (QIAGEN). Library quality control (QC) was performed using Qubit (Thermo Fisher Scientific) and TapeStation (Agilent Technologies, Santa Clara, CA, USA) and sequenced on the Illumina MiSeq platform at the DFI Microbiome Center to generate 2 × 250-bp paired-end reads.

We used dada2 1.18.0 as the default pipeline for processing MiSeq 16S rRNA reads with minor modifications in R 4.0.3 (R Foundation for Statistical Computing, Vienna, Austria). Specifically, reads were first trimmed at 190 bp for both forward and reverse reads to remove low-quality nucleotides. Chimeras were detected and removed using the default consensus method in the dada2 pipeline. Then, amplicon sequence variants (ASVs) with length between 320 bp and 365 bp were kept and deemed as high-quality ASVs. Taxonomy of the resultant ASVs was assigned to the genus level using the RDP 2.13 classifier with a minimum bootstrap confidence score of 80. Raw sequence data, ASV abundance, and taxonomy tables, in addition to bar plots, were generated.

Shotgun Metagenomic Sequencing. Libraries were prepared with 100 ng of genomic DNA using the QIAGEN QIAseq FX DNA Library Kit, with the exception of samples having low DNA yields. For samples with ultra-low DNA concentrations (10 ng or less), FX Signal Enhancer ReadyProbes Reagent (Thermo Fisher Scientific) was used. Briefly, DNA was fragmented enzymatically, and the desired insert size was achieved by adjusting fragmentation conditions. Fragmented DNA was end repaired and A's were added to the 3′ ends to stage inserts for ligation. During the ligation step, Illumina unique dual index (UDI) adapters were attached to the inserts, and the prepared library was PCR amplified. Amplified libraries were purified, and QC was performed using Agilent TapeStation. Normalized libraries were sequenced on an Illumina NextSeq 1000/2000 at the DFI Microbiome Center to generate 2 × 150-bp reads at a throughput of 5 to 10 million reads per sample.

Adapters were trimmed from the raw reads, and their quality was assessed and controlled using Trimmomatic 0.39.[28] The reads mapping to the reference human genome were identified and removed by kneaddata 0.7.10. Taxonomic classification and relative abundance estimation was performed using Kraken2 2.1.1,[29] Bracken,[30] and MetaPhlAn 4.0.2.[31] Functional analysis was performed using HUMAnN 3.8.[32] All analyses were performed using R 4.2.2 with the tidyverse 2.0.0 package.[33]

Metabolite Analysis by Mass Spectrometry

Short-Chain Fatty Acids. SCFAs were derivatized as described by Haak et al.[34] with the following modifications and analyzed by gas chromatography–mass spectrometry (GC-MS). The metabolite extract (100 µL) was added to 100 µL of 100-mM borate buffer, pH 10 (28341; Thermo Fisher Scientific), 400 µL of 100-mM pentafluorobenzyl bromide (90257; MilliporeSigma, Burlington, MA, USA) in acetonitrile (A955-4; Thermo Fisher Scientific), and 400 µL of *n*-hexane (160780010; Acros Organics, Geel, Belgium) in a capped mass spectrometry autosampler vial (09-1200; MicroLiter, Millville, NJ, USA). Samples were heated in an Eppendorf ThermoMixer C to 65°C for 1 hour while being shaken at 1300 rpm. After cooling to room temperature, samples were centrifuged at 4°C and 2000*g* for 5 minutes, allowing phase separation. From the hexanes phase (top layer), 100 µL was transferred to an autosampler vial containing a glass insert, and the vial was sealed. Another 100 µL of the hexanes phase was diluted with 900 µL of *n*-hexane in an autosampler vial. Concentrated and dilute samples were analyzed using an Agilent GC-MS (7890A GC system with 5975C MS detector) operating in negative chemical ionization mode with an Agilent HP-5ms Ultra Inert column (19091S-433UI; 30 m × 0.25 mm, 0.25 µm), methane as the reagent gas (99.999% pure), and 1-µL split injection (1:10 split ratio). Oven ramp parameters were as follows: 1 minute hold at 60°C, 25°C per minute up to 300°C with a 2.5-minute hold at 300°C. Inlet temperature was 280°C, and the transfer line was 310°C. A 10-point calibration curve was prepared with acetate, propionate, butyrate, 5-aminovalerate, glycine, proline, succinate, and tyramine, with nine subsequent 2× serial dilutions for quantitative analysis. Data analysis was performed using Agilent MassHunter Quantitative Analysis software (version B.10). Metabolite identities were confirmed by comparison of retention time and m/z to authentic standards. Normalized peak areas were calculated by dividing raw peak areas of targeted analytes by averaged raw peak areas of internal standards.

Bile Acids. BAs were analyzed using liquid chromatography–mass spectrometry.[35] The metabolite extract (75 µL) was added to prelabeled mass spectrometry

autosampler vials (09-1200; MicroLiter) and dried down completely under a nitrogen stream at 30 L/min (top) and 1 L/min (bottom) at 30°C (SPE Dry 96 Dual, 3579M; Biotage, Uppsala, Sweden). Samples were resuspended in 50:50 water:methanol (750 µL). Vials were added to an Eppendorf ThermoMixer C to resuspend analytes at 4°C and 1000 rpm for 15 minute with an infinite hold at 4°C. Samples were then transferred to prelabeled microcentrifuge tubes and centrifuged at 4°C and 20,000*g* for 15 minutes to remove insoluble debris. The supernatant (700 µL) was transferred to a mass spectrometry autosampler vial. Samples were analyzed on an Agilent 1290 Infinity II liquid chromatography system coupled to an Agilent 6546 LC quadrupole time-of-flight mass spectrometer, operating in negative mode, equipped with an Agilent Jet Stream ion source. The sample (5 µL) was injected onto an XBridge BEH C18 column (3.5 µm, 2.1 × 100 mm; Waters Corporation, Milford, MA, USA) fitted with an XBridge BEH C18 guard (Waters Corporation) at 45°C. Elution started with 72% A (water, 0.1% formic acid) and 28% B (acetone, 0.1% formic acid) with a flow rate of 0.4 mL/min for 1 minute and linearly increased to 33% B over 5 minutes, then linearly increased to 65% B over 14 minutes. The flow rate was then increased to 0.6 mL/min and B was increased to 98% over 0.5 minute, and these conditions were held constant for 3.5 minutes. Re-equilibration of the column was then completed at a flow rate of 0.4 mL/min of 28% B for 3 minutes. A 10-point calibration curve was used for quantitation of 16 bile acids (3-oxolithocholic acid, allocholic acid, alloisolithocholic acid, alpha-muricholic acid, beta-muricholic acid, chenodeoxycholic acid, cholic acid, deoxycholic acid, glycochenodeoxycholic acid, glycocholic acid, isodeoxycholic acid, lithocholic acid, taurochenodeoxycholic acid, taurocholic acid, ursocholic acid, and ursodeoxycholic acid). The electrospray ionization conditions were set with the capillary voltage at 3.5 kV, nozzle voltage at 2 kV, and detection window set to 100 to 1700 *m/z* with continuous infusion of a reference mass (Agilent ESI-TOF Biopolymer Analysis reference mix) for mass calibration. A 10-point calibration curve was used for quantitation. Data analysis was performed using Agilent MassHunter Quantitative Analysis software (version B.10). Metabolite identities were confirmed by comparison of retention times, *m/z* ratios, and fragmentation patterns to authentic standards. Normalized peak areas were calculated by dividing raw peak areas of targeted analytes by averaged raw peak areas of internal standards.

Genetic Testing. The Macula Risk test reports on the presence of 14 single nucleotide polymorphisms (SNPs) on 12 genes of interest that have been linked to the development of AMD, including *CFH*, *CFI*, *C3*, *C2*, *CFB*, *LIPC*, *ABCA1*, *CETP*, *COL8A1*, *APOE*, *TIMP3*, and *ARMS2*.[26,27,36,37] DNA was isolated from each patient's buccal swab specimen, and the 14 genetic regions associated with AMD were amplified using PCR. Allele-specific primer extension was performed for SNP determination using the MassARRAY System (Agena Bioscience, San Diego, CA, USA), and genotypes were assigned. The reported genotype represents the combination of alleles that each subject had at that particular genomic position inherited from both parents. The presence of a minor allele at an SNP is indicative of genetic variation and is positively correlated with increased risk. If a patient is found to have no copy of the minor allele, that SNP is considered to represent a low risk for contributing to the development of AMD; one copy of the minor allele indicates intermediate risk, and two copies of the minor allele from both parents are indicative of high risk compared to individuals with other genotypes.[27]

Statistical Analysis

The raw ASV counts were normalized by relative abundance and center-log transformation (CLR) using the R packages phyloseq and ALDEx2.[38,39] Alpha diversity metrics of observed operational taxonomic units (OTUs), Shannon index, Simpson index, evenness, and genus number were used from the phyloseq1 library to dissect the complexity within each sample. The two-sided pairwise *t*-test was used to estimate the difference for contrast groups of control versus intermediate, intermediate versus advanced, and control versus advanced. Beta diversity was based on principal coordinate analysis (PCoA) of the Euclidean distance between CLR-normalized microbiome compositions. Multivariate statistical tests of permutational multivariate analysis of variance (PERMANOVA) were used to measure significance on the compositional difference among the three groups. The beta diversity of all 16S samples was visualized on the top two principal coordinates analysis (PCoA) dimensions, highlighting the separation for the three AMD groups. Significant changes in ASV abundance were assessed using edgeR on relative log expression normalized counts aggregated on multiple taxonomy levels, and taxa exhibiting a false discovery rate (FDR)-adjusted $P < 0.05$ were considered significant.[40]

The box plots of relative abundance demonstrate the microbiome variation among the three groups for selected taxa. Analysis of metabolomics data was performed in R using one-sided Wilcoxon rank-sum tests without assumption of normality in a pairwise fashion to compare concentrations of control to intermediate AMD, control to advanced AMD, and intermediate AMD to advanced AMD. $P < 0.05$ was considered statistically significant. Genetic association analyses were conducted by comparing frequencies of each risk allele between intermediate and advanced AMD cohorts using Fisher's exact test. Multiple testing was corrected using the Benjamini–Hochberg procedure, and Haldane–Anscombe correction was utilized to circumvent values of zero when calculating odds ratios of risk alleles between cohorts.

Pathway abundance was identified using HUMAnN, and the normalized copies per million (CPM) was used as the relative abundance metric (here, CPM is analogous to transcripts per million [TPM] used in RNAseq). Most significantly different pathways were identified using the Kruskal–Wallis rank-sum test with $P < 0.05$, and the Wilcoxon rank-sum test was used for each comparison.

Results

Study Demographics

To investigate the association of intestinal microbiome with the occurrence of AMD, we analyzed the gut microbiota of 16 patients with clinically confirmed AMD and six healthy age- and sex-matched controls. AMD patients and controls were similar with regard to age at sample collection, body mass index (BMI), sex, smoking habit, race, and best-corrected visual acuity (BCVA) (Table 1). Snellen visual acuity (VA) measurements were converted to logarithm of the minimum angle of resolution (logMAR) VA for standardized inter-

Table 1. Characteristics of Study Patients

Feature	Control ($n = 6$)	Intermediate ($n = 8$)	Advanced ($n = 8$)	*P*
Age (y), mean ± SD	76.3 ± 8.8	75.9 ± 4.9	79.1 ± 7.2	0.61*
Male, *n* (%)	2 (33.3)	4 (50.0)	4 (50.0)	0.76†
BMI (kg/m^2), mean ± SD	28.5 ± 5.0	28.8 ± 4.4	27.1 ± 5.6	0.79*
Smoker, *n* (%)	1 (16.7)	3 (37.5)	3 (37.5)	0.72†
VA (logMAR), mean ± SD	0.27 ± 0.21	0.21 ± 0.18	0.45 ± 0.46	0.30*
Race, *n* (%)				0.06†
Black	2 (33.3)	0 (0.0)	0 (0.0)	
White, non-Hispanic	4 (66.7)	8 (100.0)	8 (100.0)	

Smoker feature includes current smokers and previous smokers.
* ANOVA.
† Fisher's exact test.

Table 2. SNPs in AMD

Gene	SNP	A1	A2	F_Adv	F_Int	*P*	OR	95% CI	FDR BH
CFH	rs3766405	C	T	0.63	1.00	0.02	0.05	(0–1.04)	0.28
	rs412852	C	T	0.56	0.94	0.04	0.09	(0.01–0.82)	0.28
ABCA1	rs1883025	C	T	0.63	0.94	0.08	0.11	(0.01–1.07)	0.37
APOE	rs429358	T	C	0.94	0.69	0.17	6.82	(0.69–66.9)	0.60
	rs7412	T	C	0.19	0.25	1.00	0.69	(0.13–3.76)	1.00
ARMS2	372_815del443ins54	D	N	0.25	0.38	0.75	0.56	(0.12–2.54)	1.00
C2	rs9332739	G	C	1.00	1.00	1.00	1.00	(0.02–53.55)	1.00
C3	rs2230199	G	C	0.19	0.31	0.69	0.55	(0.11–2.83)	1.00
CETP	rs3764261	A	C	0.44	0.56	0.72	0.6	(0.15–2.45)	1.00
CFB	rs541862	A	G	1.00	0.94	1.00	2.13	(0.07–68.36)	1.00
CFI	rs10033900	T	C	0.75	0.63	0.7	1.8	(0.39–8.22)	1.00
COL8A1	rs13095226	T	C	0.75	0.81	1.00	0.69	(0.13–3.75)	1.00
LIPC	rs10468017	C	T	0.81	0.69	0.69	1.97	(0.38–10.17)	1.00
TIMP3	rs9621532	A	C	0.94	1.00	1.00	0.47	(0–15.02)	1.00

A1, minor allele; A2, major allele, F_Adv, frequency of A1 in advanced AMD; D, deletion; F_Int, frequency of A1 in intermediate AMD; N, normal; OR, odds ratio for A1, FDR BH, rate correction using the Benjamini–Hochberg procedure. P values were calculated with the Fisher's exact test and are for comparisons of allele frequencies between advanced and intermediate cohorts.

vals. In total, eight AMD patients were determined to be in the advanced stage (three with GA and five with exudative AMD), and eight patients were in the intermediate stage.

Genetics

Genetic information was collected only for the enrolled AMD patients (advanced, $n = 8$; intermediate, $n = 8$). After correction, none of the 14 tested genetic polymorphisms was present at significantly different frequencies between the intermediate and advanced AMD cohorts (Table 2).

16s: Taxonomic Characterization of Gut Microbiome

Following 16s rRNA sequencing of stool samples and data normalization using relative abundance, the advanced cohort demonstrated a significantly greater alpha diversity than the intermediate cohort, as well as marginally significant beta diversity separation compared to the control group (Figs. 1A, 1B). The phylum Firmicutes was found to dominate the microbiome composition in all cohorts, with Clostridia, Erysipelotrichia, and Bacilli among the most abundant classes within this phylum (Figs. 2A, 2B). Bacilli was found to be significantly more abundant in the intermediate cohort compared to controls (FDR = 0.046) and the advanced group (FDR = 0.034). However, at the class level, Clostridia and Erysipelotrichia were not found to differ significantly between groups. At the order level, the advanced group had a marginally significant increase in relative abundance of Desulfovibrionales compared to controls (FDR = 0.114) and the intermediate group (FDR = 0.102) (Fig. 3). Although the relative abundance of order Clostridiales was not significant between groups, the advanced group had significantly higher abundance of several key taxa within this order compared to the intermediate group. These included the families *Peptococcaceae* (FDR = 0.021) and *Gracilibacteraceae* (FDR = 0.031), and the genera *Butyrvibrio* (FDR = 0.012), *Lachnotalea* (FDR = 0.017), *Paludicola* (FDR = 8.90e-03), and *Terrisporobacter* (FDR = 1.16e-03) (Figs. 4, 5).

Fecal Metabolomics

Targeted quantitative and qualitative metabolomic analysis of various fecal SCFAs and bile acid metabolites were performed. A heatmap was plotted using $\log_2$ fold changes relative to the median value of the compound (Fig. 6).

Short-Chain Fatty Acids. As products of gut bacteria fermentation pathways, SCFAs are used as fuel for gut epithelial cells. Recent findings, however, show that SCFAs also have important roles in immunomodulatory functions.[36] Among our subjects, seven key SCFAs were found to be in significantly lower concentrations in the advanced group compared to the intermediate group. These included

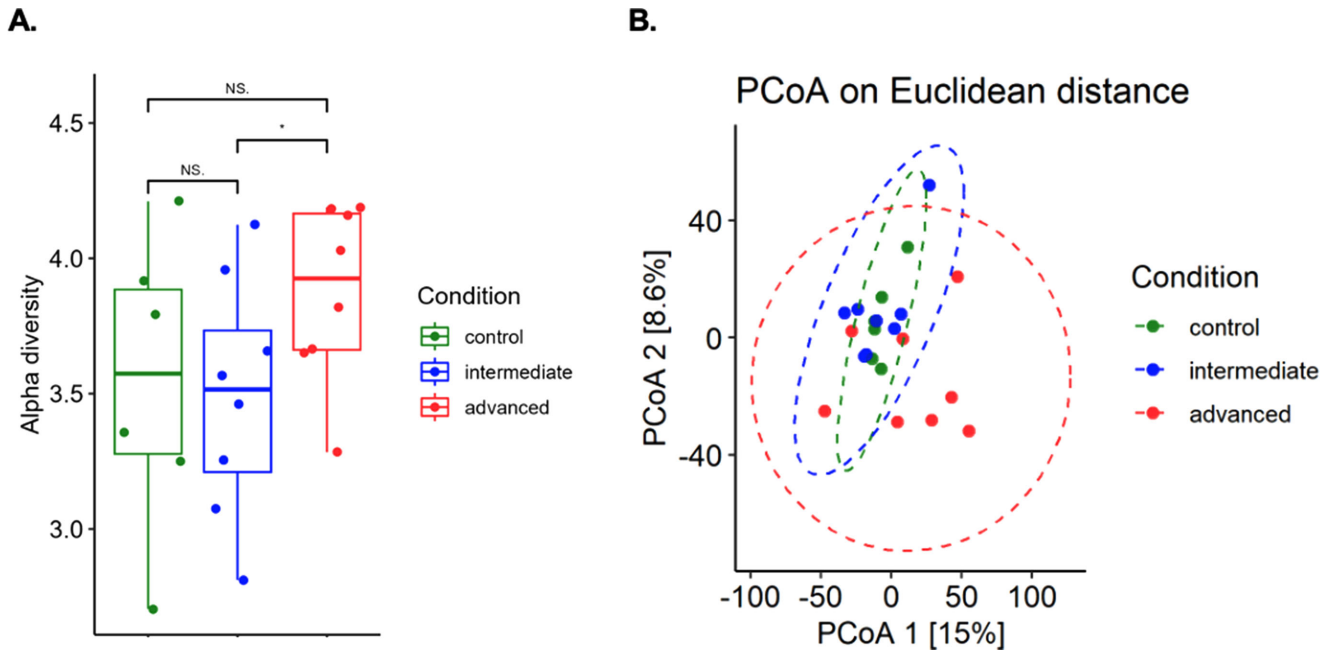

Figure 1. Bacterial diversity between cohorts. (**A**) Alpha diversity metrics of the Shannon index showed increased alpha diversity in the advanced cohort compared to intermediate ($P = 0.049$). (**B**) Beta diversity of all 16S samples was visualized on the top two PCoA dimensions using health status as a grouping variable. Separation between controls and advanced cohort was found to be near significant ($P = 0.086$).

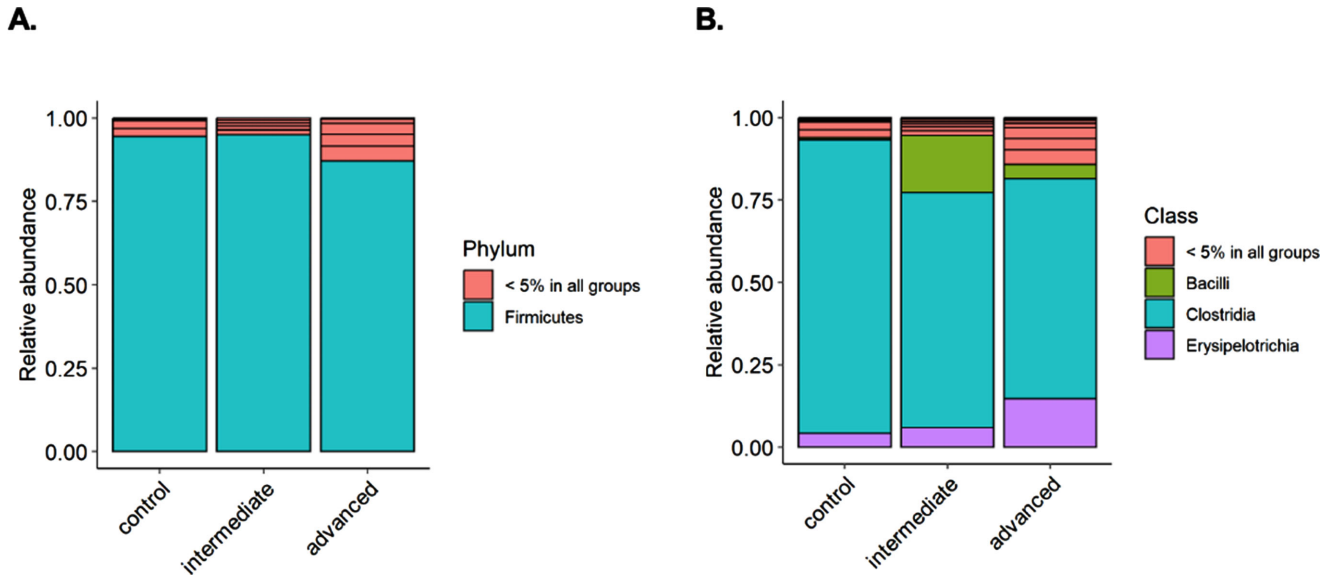

Figure 2. Aggregated relative abundances of microbiome composition. (**A**) Phylum Firmicutes was the most abundant across all three cohorts (94.3% in controls, 94.9% in intermediate, and 87.0% in advanced). (**B**) Class Clostridia had the greatest relative abundance in all groups (89.0% in controls, 71.3% intermediate, and 66.8% in advanced) followed by Erysipelotrichia (4.2% in controls, 6.0% in intermediate, and 14.7% in advanced).

2-methylbutyrate ($P = 0.04$), acetate ($P = 0.002$), butyrate ($P = 0.04$), isobutyrate ($P = 0.02$), isovaleric acid ($P = 0.04$), phenylacetate ($P = 0.01$), and propionate ($P = 0.01$) (Fig. 7). Of these, 2-methylbutyrate ($P = 0.03$), isobutyrate ($P = 0.02$), isovaleric acid ($P = 0.04$), and phenylacetate ($P = 0.001$) were also elevated in the intermediate AMD group relative to the control cohort. 5-Aminovalerate ($P = 0.01$) was greatest in controls. Additional differentially expressed metabolites can be found in Supplementary Figure S1.

Bile Acids. Several other classes of gut microbiota-associated metabolites have been shown to be powerful signaling molecules and are being studied for their role in modulating neurologic and retinal diseases, among them BAs.[41] We found that the control group had higher concentrations of key primary BAs compared to patients with advanced AMD, including taurochenodeoxycholic acid (TCDCA) ($P = 0.001$) and taurocholic acid (TCA) ($P = 0.001$), as well as key secondary BAs such as taurolithocholic acid

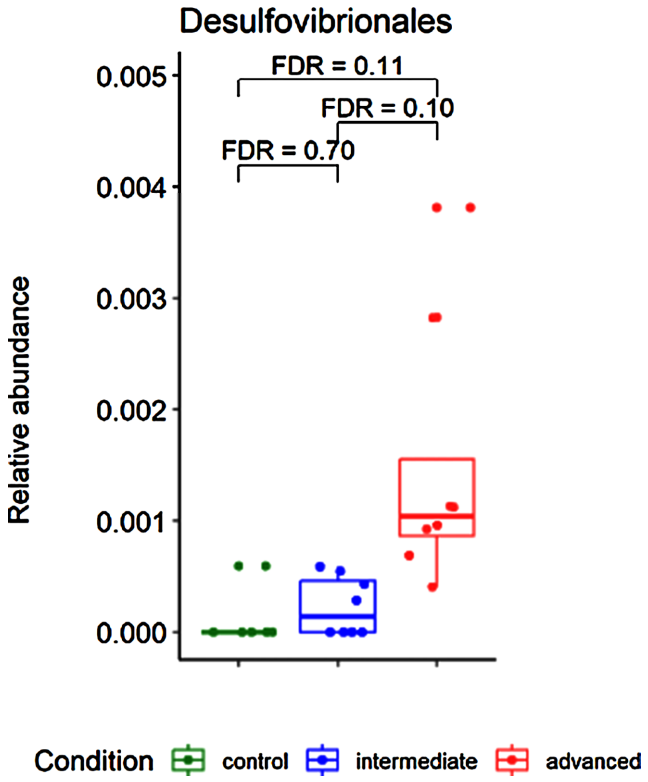

Figure 3. Relative abundance difference at the order level. Box plot represent the mean ± SD abundance of bacterial orders associated with AMD (PERMANOVA). Desulfovibrionales of class Deltaproteobacteria was greater with marginal significance in the advanced group compared to controls (logFC = 2.50) and the intermediate group (logFC = 1.70).

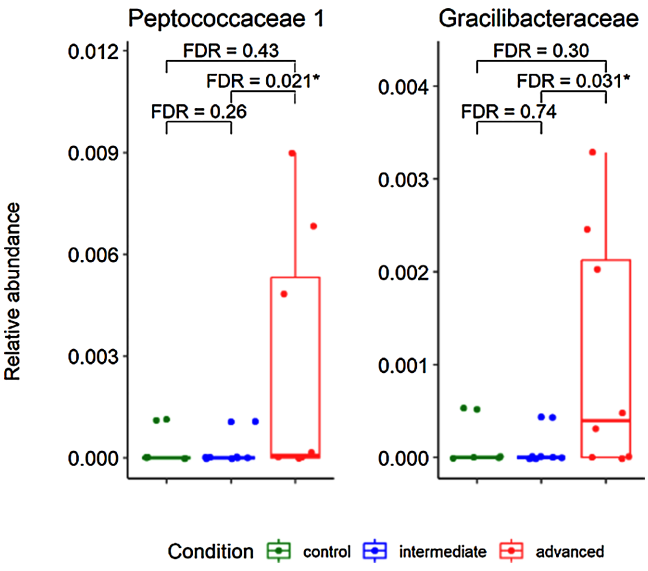

Figure 4. Relative abundance difference at the family level. Box plots represent the mean ± SD abundance of bacterial families associated with AMD (PERMANOVA, FDR < 0.05). *Peptococcaceae* (logFC = 3.47) and *Gracilibacteraceae* (logFC = 2.67) of class Clostridia were both greater in the advanced group compared to the intermediate group.

(TLCA) (P = 0.001), taurodeoxycholic acid (TDCA) (P = 0.002), tauroursodeoxycholic acid (TUDCA) (P = 0.006), and tauro-alpha or tauro-beta muricholic acid (TαMCA/TβMCA) (P = 0.01). TCA, TDCA, TUDCA, and TαMCA/TβMCA were also found in greater concentrations in the intermediate cohort compared to the advanced AMD group (Fig. 8).

Functional Profiling of Gut Microbiota

To describe the microbial functional profiles, we applied HUMAnN on each sample and assessed the relative abundance of functional pathways assigned based on organism-specific gene hits.[25] From the total 2611 assigned organism-specific pathways and 466 aggregated pathways, 13 abundant pathways were screened to significantly differ between cohorts (Fig. 9). The superpathway of glycolysis integrated with the Entner–Duodoroff pathway was upregulated in the intestinal microbiome of advanced AMD patients compared to controls (P = 0.013), whereas galactitol degradation (P = 0.003), superpathway of hexitol degradation (P = 0.008), hexitol fermentation (P = 0.043), formaldehyde fermentation (P = 0.003), and guanosine nucleotide degradation (P = 0.043) pathways were enriched in the microbiome of controls. Advanced AMD patients also had a decrease in bacterial genes connected to the non-oxidative branch of the pentose phosphate pathway (P = 0.01), hexitol fermentation (P = 0.005), pyruvate fermentation (P = 0.038), D-galactose degradation (P = 0.01), guanosine nucleotides degradation (P = 0.005), dTDP–*N*-acetylthomosamine biosynthesis (P = 0.018), purine ribonucleosides degradation (P = 0.021), and L-tryptophan biosynthesis (P = 0.002) compared to intermediate AMD patients.

Discussion

In this study, we identified several novel differences in gut microbiome composition and metabolite concentrations that associate with AMD disease status. In particular, we found that patients with advanced AMD had increased abundance of order Desulfovibrionales compared to intermediate AMD cases and controls. An increased presence of Desulfovibrionales has been linked to diets high in saturated fat (Western diet) and has been implicated in several non-infectious systemic diseases ranging from ulcerative colitis to ankylosing spondylitis through damaging DNA, inhibiting lysozyme enzymatic functions in the gut microenvironment, and blocking mitochondrial respiration.[42–44] Most notable has been its strong link to the development of Parkinson's disease through induction of the oligomerization and aggregation of α-synuclein protein.[45] In retinal diseases, such as diabetic retinopathy and AMD, clinical studies have highlighted dysregulation of Desulfovibrionales compared to healthy controls.[46,47] Polysaccharides derived from Desulfobacterota generate inflammatory injuries, trigger abnormal equilibrium of metabolism, and inhibit endotoxin tolerance, all of which are related to the pathogenesis of retinopathy. An order of sulfate-reducing anaerobic bacteria, Desulfovibrionales, is also known to produce toxic hydrogen sulfide, which can compromise gut barrier function by directly reducing mucosal thickness.[48] Compromised gut epithelium due to hydrogen sulfide can also result in increased circulating gut microbial products such as lipopolysaccharides, peptidoglycan, or SCFAs that have been shown to activate proinflammatory Th1 and Th17 adaptive

Investigative Ophthalmology & Visual Science

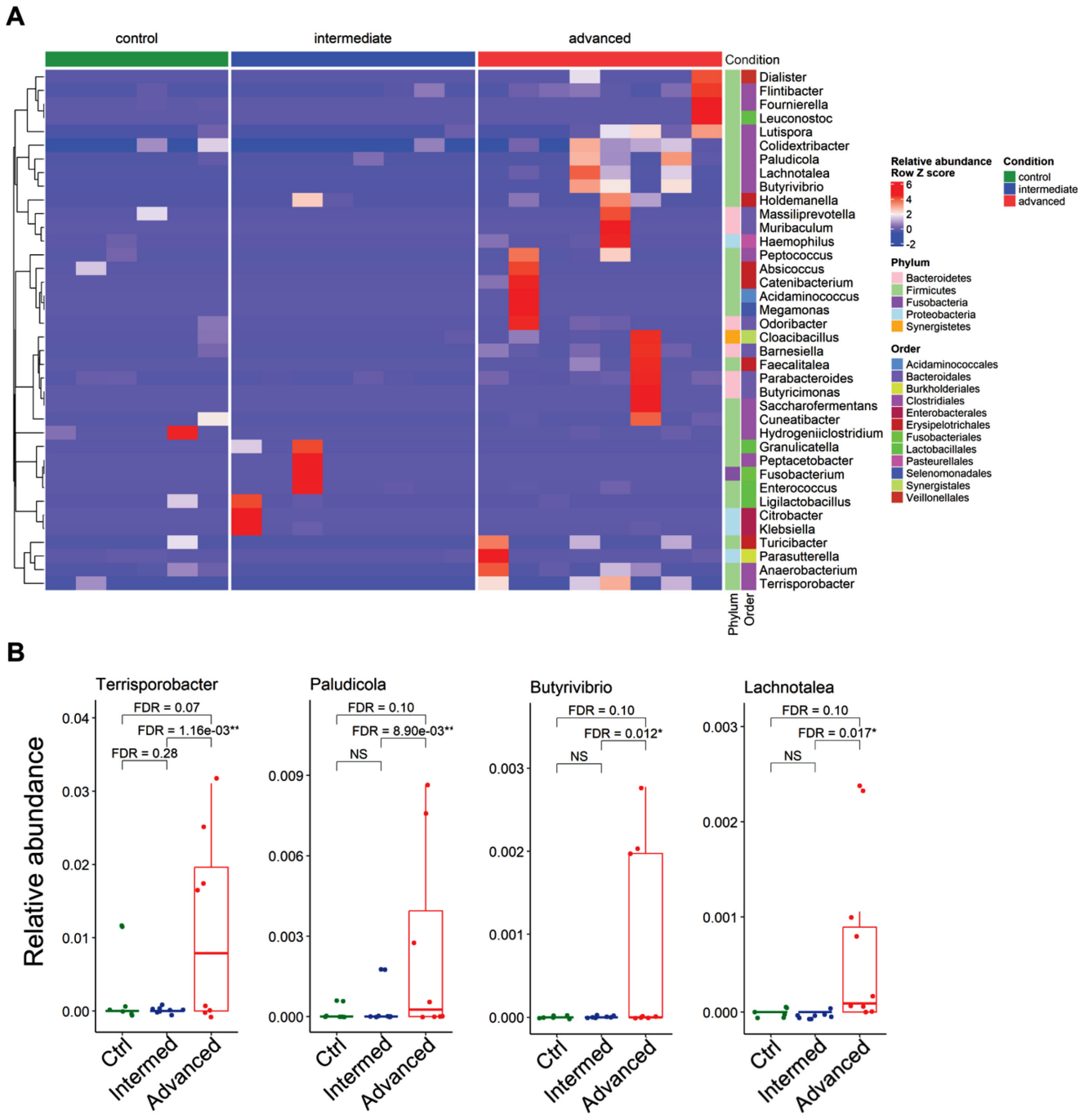

Figure 5. Relative abundance difference at the genus level. (**A**) Hierarchical clustering of bacterial genera among controls and intermediate AMD and advanced AMD patients. A total of 43 differentially abundant genera were identified with FDR < 0.05. *Red* and *blue* indicate upregulated and downregulated genera, respectively. (**B**) Box plots represent the mean ± SD abundance of key bacterial genera associated with AMD (PERMANOVA, FDR < 0.05). Within class Clostridia (logFC = 1.38), *Terrisporobacter* of family *Peptostreptococcaceae* (logFC = 6.93), *Paludicola* of family *Ruminococcaceae* (logFC = 4.31), and *Butyrivibrio* (logFC = 3.59) and *Lachnotalea* (logFC = 3.15) of family *Lachnospiraceae* (logFC = 3.59) were all significantly greater in the advanced group compared to the intermediate group and marginally significant compared to controls.

immunity pathways and lead to the onset of various inflammatory ocular diseases, such as uveitis, diabetic retinopathy, and AMD.[43,46,47]

Advanced AMD patients also had significant increased abundance of several taxa within the Clostridia class, including the families *Peptococcaceae* and *Gracilibacteraceae* and genera *Butyrvibrio*, *Lachnotalea*, *Paludicola*, and *Terrisporobacter* compared to intermediate AMD and controls. Current literature suggests that these taxa potentially represent a cluster of major immune activity via downregulation of IL-12B and upregulation of IL-4.[49] The presence of *Terrisporobacter* has even been implicated in the autoimmune disease rheumatoid arthritis.[50] Furthermore, these bacteria all belong to the order Clostridiales, which

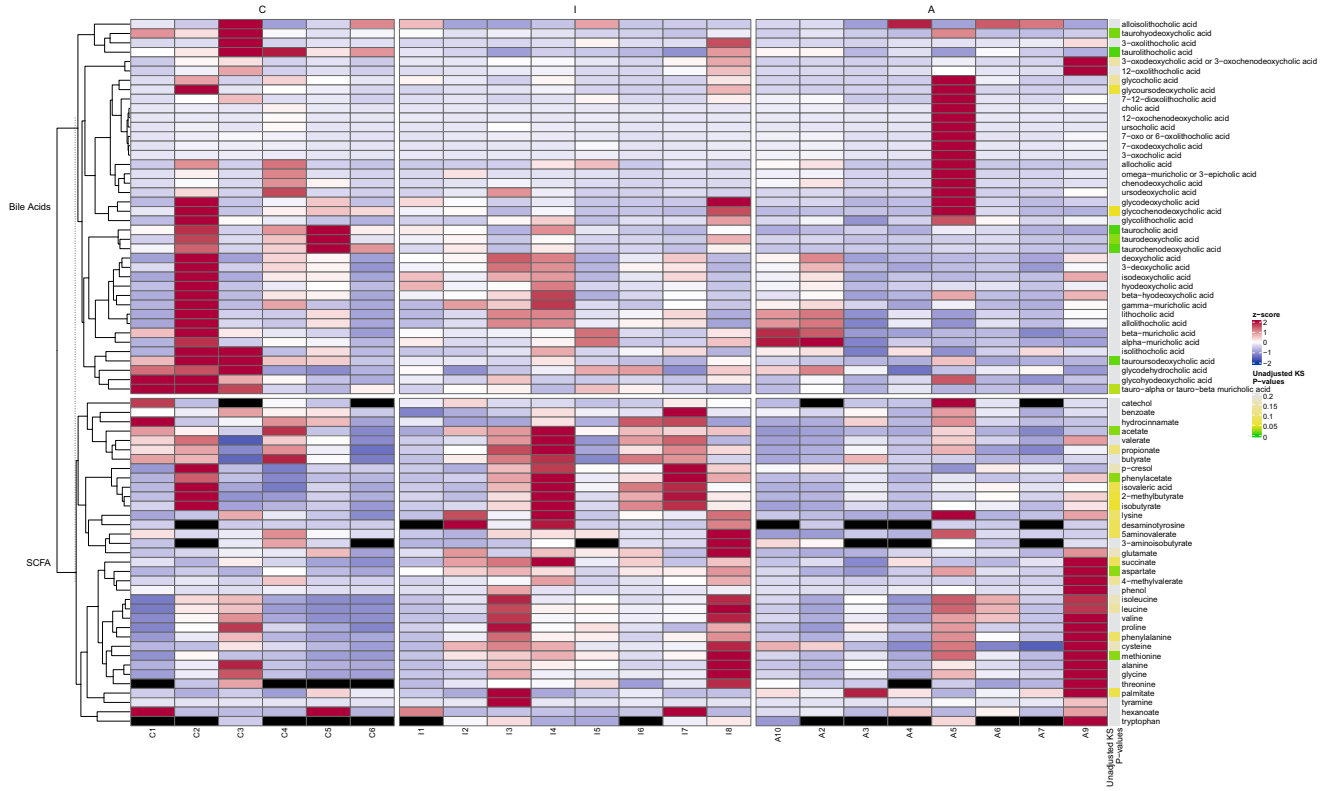

Figure 6. Heatmap of relative abundance of SCFAs and BA metabolites in fecal samples of controls (C), intermediate AMD (I), and advanced AMD (A). Normalized quantities were calculated according to the median value of that metabolite, ranging from −2 (*blue*) to +2 (*red*) in row *z*-scores. *Black* indicates not detected.

has been linked to retinal disease. Specifically, Rowan et al.[13] induced AMD-like features using a high-glycemic diet in mice and showed that the presence of microbiota belonging to Clostridiales was associated with the high-glycemic diet–induced retinal changes that mimicked advanced dry AMD.

Our findings indicate a lower representation of Bacteroidetes (<5% across all groups) compared to other human gut microbiome studies, potentially reflecting methodological differences or specific cohort characteristics. Rigorous sample collection and preservation protocols were applied to enhance the reliability of our microbial profiles. Samples were promptly processed and stored at −80°C to minimize compositional shifts, and multiple analytical approaches were used to ensure robustness in taxonomic patterns. Morning collection of all samples, as detailed in the results, may have influenced composition due to circadian effects on the gut microbiome.[51–54]

Beyond the microbiota–metabolic associations with AMD, certain microbiota may be related to the genetic susceptibility of this disease. Polymorphisms of genes involved in complement signaling, such as complement factor H (*CFH*) and complement component 3 (*C3*), are strongly implicated with differential risk for AMD development and progression.[37,55,56] Involved in mediating immune function, genetic variants of these proteins can lead to dysregulation of the complement system and promotion of retinal inflammation.[57,58] For example, Zysset-Burri et al.[17] analyzed the gut microbiomes of C3-deficient and wild-type mice in terms of taxonomic and functional profiles. They found that C3-deficient mice had enriched Firmicutes and expression of genes involved in the 5-aminoimidazole ribonucleotide biosynthesis pathway, an intermediate molecule implicated in AMD pathogenesis. Furthermore, clinical metadata was used to demonstrate positive correlation of SNPs within the *CFH* gene with the taxa Negativicutes and Clostridiales, both of which serve as potential biomarkers for AMD.[17] In our study, however, we did not find significant differences in the frequency of high-risk alleles associated with AMD between our intermediate and advanced disease cohorts. The SNPs with the two lowest p-values (Benjamini-Hochberg corrected $q = 0.28$) were rs3766405 and rs412852, both within the CFH gene, and have been shown to contribute to a small portion of AMD progression rate from intermediate to advanced.[56,59] Additionally, while *CFH* variants have been associated with alterations of gut microbiota in the literature, such studies were limited in comparing controls to subjects with general disease phenotype and did not discriminate between severity. Our findings suggest that the gut microbial differences present between the intermediate and advanced AMD groups in our study cohort are likely driven more by environmental factors than genetic susceptibility though this is a pilot study, and larger confirmatory studies are needed as small sample sizes may be masking potentially significant differences.

Metabolomics

Gut microbiota-derived metabolites play diverse roles in regulating nutrient metabolism, immune function, and angiogenesis.[18,60,61] Using targeted metabolite panels, we found seven protective SCFAs were significantly reduced

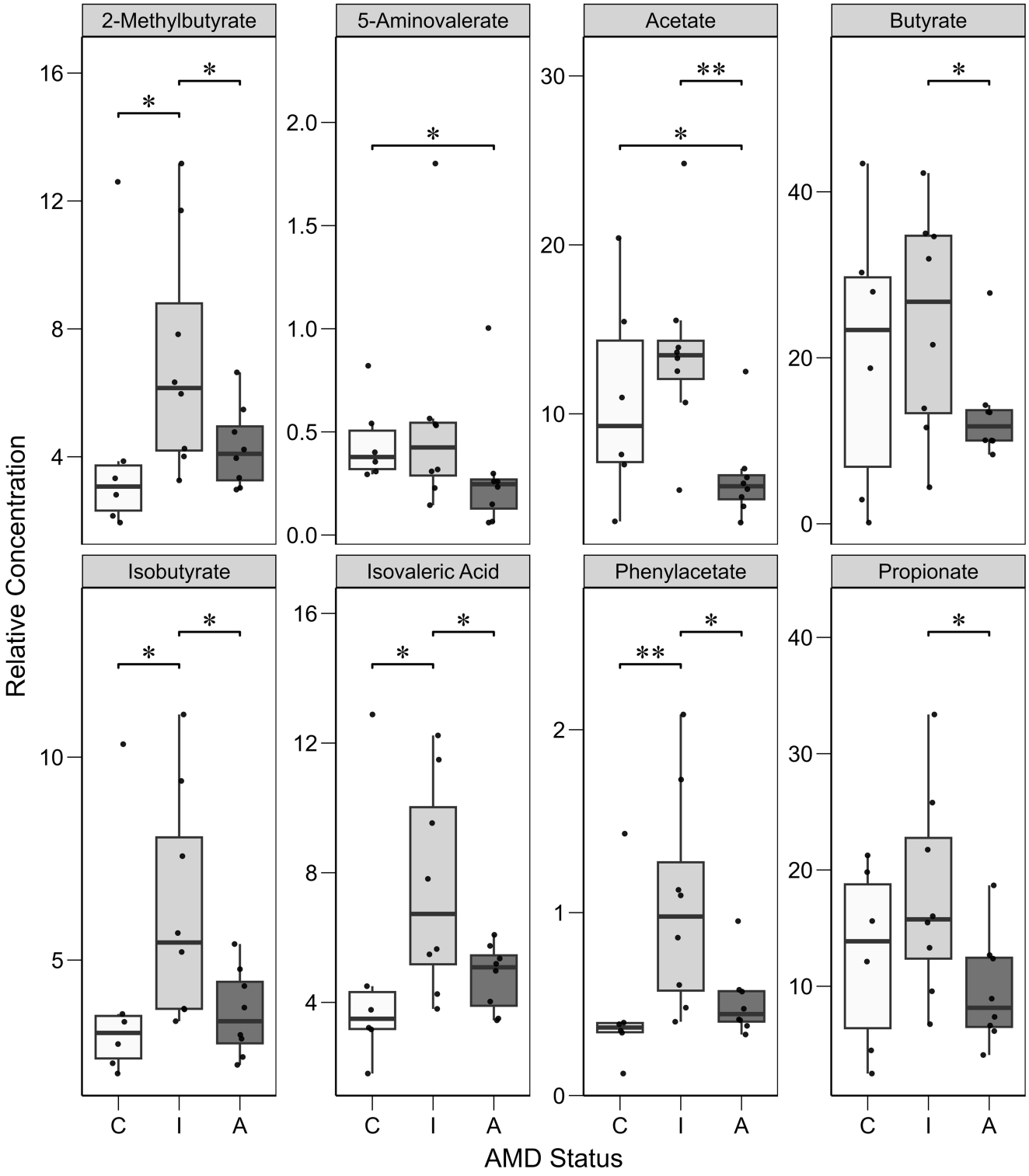

Figure 7. SCFA concentrations from fecal samples. Box plots represent the mean abundance of key short chain fatty acids. 5-Aminovalerate, acetate, butyrate, and propionate were lowest in advanced patients. 2-Methylbutyrate, isobutyrate, isovaleric acid, and phenylacetate were in greatest abundance in intermediate patients compared to both controls and advanced. Statistical significance was determined using the non-parametric Wilcoxon rank-sum test. *$P < 0.05$, **$P < 0.01$.

in the advanced cohort compared to intermediate AMD patients: acetate, propionate, butyrate, isobutyrate, 2-methylbutyrate, phenylacetate, and isovaleric acid (Fig. 7). Acetate, propionate, and butyrate constitute over 95% of SCFAs in humans.[62] Among many neurologic cell types that respond to SCFA signaling, CNS microglia have been shown to rely on the SCFA acetate for proper maturation, phagocytic function, and metabolism. Deficiency of acetate results

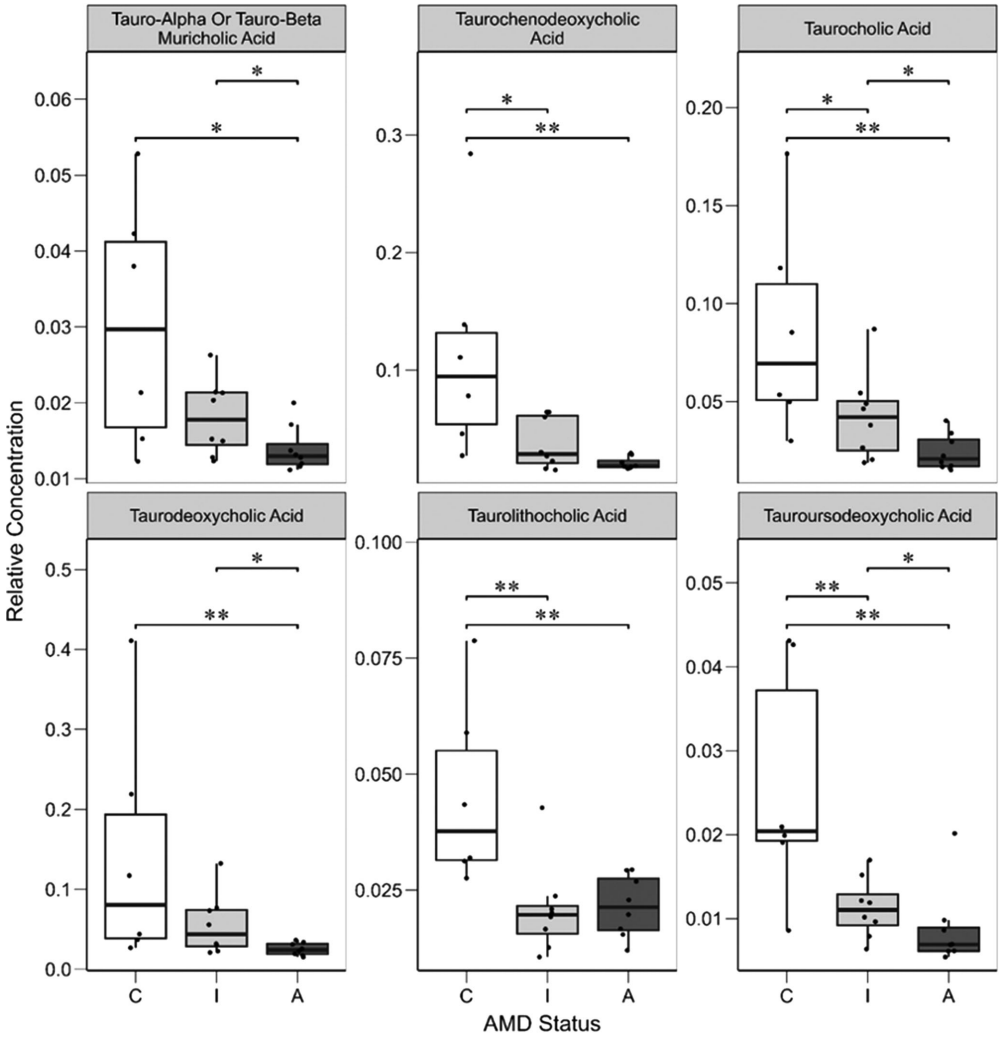

Figure 8. Bile acid concentrations from fecal samples. Box plots represent the mean abundance of bile acids: TαMCA/TβMCA, TCDCA, TCA, TDCA, TLCA, and TUDCA. Statistical significance was determined using the non-parametric Wilcoxon rank-sum test. *$P < 0.05$, **$P < 0.01$.

in dysfunctional microglia that are characteristic of neurodegenerative states.[63] Because SCFAs can cross the blood-brain barrier and regulate signaling between the gut and the brain, changes in their normal levels is linked with several neurologic diseases a perspective in the brain that may also be applicable to the blood retina barrier.[63,64] In this regard Horai et al.[65] showed that a population of retina-specific CD4+ T cells were trained through their interactions with the gut microbiome in a mouse model of uveitis. While the mechanism underlying these interactions is unclear, the signaling provided by SCFAs may be important in dampening pathologic ocular inflammation, as oral administration of acetate, propionate, or butyrate has been shown to modulate the severity of uveitis in mice by altering immune-trafficking of effector T cells and induction of regulatory T cells.[66]

Beyond regulation of host immunity and metabolism at gut-level interactions, studies also point to direct effects of SCFAs in ocular tissue, affecting nearly all cellular components of the retina. The wet form of advanced AMD is characterized by choroidal neovascularization (CNV). SCFAs have been shown to be anti-angiogenic; for example, in laser-induced mouse models of CNV, administration of butyrate reduces CNV lesion size, which is supported by in vitro evidence of decreased VEGFA and VEGFR2 signaling.[67,68] Recent studies have begun looking into optimizing the delivery of butyrate in nanoparticles as a potential modality of treating nAMD,[69] a concept that goes beyond the scope of our study.

Interestingly, we found that isomers of these SCFAs isobutyrate and isovaleric acid, as well as functionally similar compounds such as 2-methylbutyrate and phenylacetate, were highest in intermediate patients but had similar concentrations in controls and advanced. Although their exact roles are less known, this discrepancy may suggest their ineffectiveness in serving as biomarkers for AMD disease progression, although further studies would be necessary to validate this finding.

In addition to SCFAs, we determined that the control group had greater concentrations of protective conjugated BAs, including conjugated primary bile acids TCA and TCDCA, along with conjugated secondary bile acids TLCA, TUDCA, TDCA, and TαMCA/TβMCA (Fig. 8). Many detailed studies have identified functional and molecular changes of retinal cell types in response to these specific

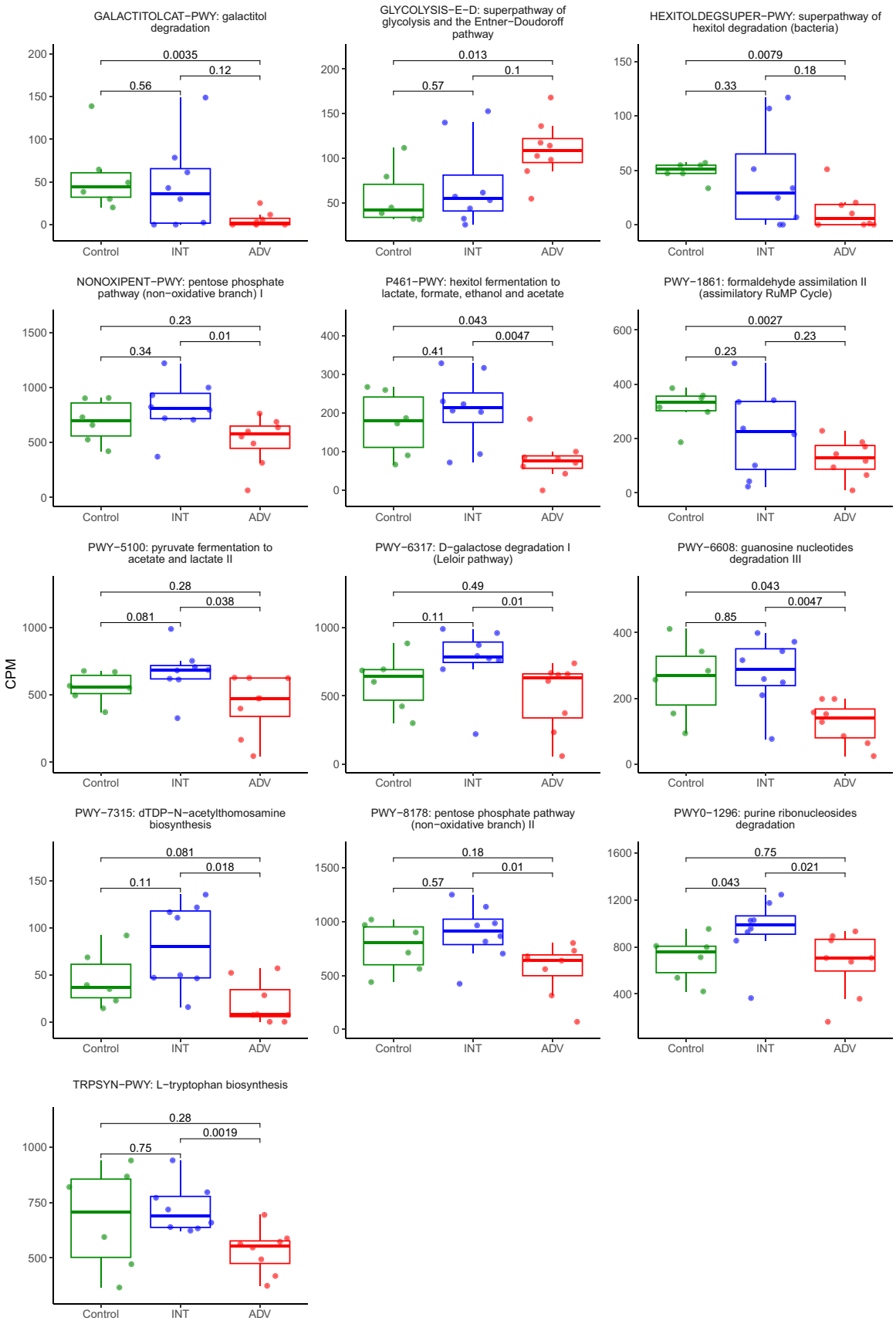

Figure 9. Species-specific microbial pathways associated with AMD. Box plots represent the mean ± SD relative abundance of 13 metabolic pathways differentially abundant between cohorts (Wilcoxon rank-sum test). *Green* represents controls ($n = 6$), *blue* represents intermediate AMD ($n = 8$), and *red* represents advanced AMD patients ($n = 8$).

Investigative Ophthalmology & Visual Science

BA signals. TCA has shown to inhibit features of AMD in vitro, promoting RPE integrity and decreasing VEGF-induced choroidal endothelial migration.[70] TCDCA has been shown to inhibit astrocyte inflammation by downregulating mRNA expression of inflammatory genes such as cyclooxygenase 2 (*COX2*), tumor necrosis factor-α (*TNF-α*), and *IL-6* likely through TGR5-mediated nuclear factor kappa B (NFκB) signaling.[71] TαMCA/TβMCA are natural farnesoid X receptor (FXR) antagonists and therefore regulate pathways involved in lipid metabolism, energy homeostasis, and inflammation.[72] TUDCA, a neuroprotective BA, appears to affect multiple age-related processes, including reducing age-dependent accumulation of amyloid in the brains of mice.[73] Additionally, TUDCA reduces human endothelial cell proliferation and has been shown to protect against retinal degeneration and diabetic retinopathy.[74–76] Regarding clinical data, in a case–control study with 85 AMD subjects by Kiang et al.,[77] metagenomics analysis showed that control patients demonstrated enrichment in microbial pathways of both primary and secondary bile acid synthesis, as well as peroxisome proliferator-activated receptor (PPAR) signaling, which is important in maintaining RPE and overall retinal health.[77] This finding has been corroborated by another metabolomics study, demonstrating lower levels of bile acids in serum of patients with nAMD.[78] These studies, coupled with our data, suggest that BAs may serve a modulatory role in AMD pathology, though further study is required.

Metabolic Pathways

Functional annotation analysis indicated that genes involved in metabolic pathways related to carbohydrate and nucleotide metabolism were differentially expressed between our cohorts (Fig. 9). Regarding carbohydrate metabolism and assimilation, advanced AMD patients had an increase in bacteria responsible for the Entner–Doudoroff (ED) pathway and a decline in pathways of galactitol and hexitol degradation, formaldehyde assimilation, pentose phosphate pathways, and the fermentation of pyruvate and hexitol to acetate and lactate end products compared to other groups. Chronic oxidative stress redirects glucose catabolism in various microbes by inhibiting key enzymatic pathways.[79] For example, many virulent microorganisms such as *Entamoeba histolytica* and *Salmonella enterica* show an increased dependency on fatty acids and acetate utilization by the enriched ED pathway.[79,80] The increase of the ED pathway among our advanced AMD cohort, along with the reduction in fermentation of pyruvate and hexitol to lactate and acetate end products, correlates with the decreased presence of acetate and other protective SCFAs among these patients.

Advanced AMD patients also demonstrated a decrease in degradation pathways of various sugar compounds. Sugars in excess are converted to polyols by lens aldose reductase and have been implicated in diabetic hyperglycemia-associated abnormalities and retinal vascular changes due to degeneration of capillary pericytes.[81–83] Furthermore, galactose and other monosaccharides can auto-oxidize under physiological conditions and form dicarbonyl compounds and hydrogen peroxide, both of which are toxic and have been linked to the formation of early cataracts.[84]

Moreover, intestinal microbiomes of the intermediate AMD patients were enriched in genes of purine ribonucleoside degradation but advanced AMD patients showed a decrease in guanosine nucleotide degradation compared to controls. Anomalous purine signaling pathways have been linked to the development of various autoimmune diseases through immune dysregulation and consequent antibody production.[85] Although autoimmunity and the generation of autoantibodies are associated with ocular diseases including AMD, the specific triggers for ocular autoimmunity remain unidentified. In a previous study comparing functional features between control and AMD cohorts, Zysset-Burri and associates[17] also found that pathways of purine ribonucleoside degradation were elevated in fecal samples of AMD patients, suggesting that immune dysregulation in AMD may occur via abnormal purine signaling. Finally, advanced AMD patients had a significant decrease in bacteria responsible for L-tryptophan biosynthesis. L-Tryptophan is an essential component of the human diet that induces long-term immune tolerance, and alterations in its metabolism have been linked to states of hyperinflammation.[86,87]

As a pilot study, our objectives focused on investigating shifts in gut microbiome composition and metabolomic profiles across different AMD disease states. This study has not established direct causal links between altered intestinal microbiota and AMD onset or progression. Key limitations include a small sample size, which restricts the ability to confirm consistent differences across groups, the absence of longitudinal data, the lack of genetic data for control patients, and limited statistical testing of metabolomic data without adjustments for multiple comparisons. Additionally, the relatively older age of participants across groups may not fully represent the wider AMD population. Potential confounding factors include coexisting systemic diseases and dietary differences between patients and controls. Finally, general limitations of studying the microbiome using stool samples include the inherent heterogeneous composition of stool, making the samples susceptible to changes during collection and processing. Consequently, the microbiome profiles may be misrepresented due to subsampling of incompletely homogenized stool, which can lead to variations in bacterial abundance and can be exacerbated in metabolomic analyses.

Conclusions

The differential abundance of specific orders and genera within major bacterial classes may serve as a means of identifying key players in the pathogenesis of advanced AMD. Although the findings may have been limited by low power, the presence of a higher diversity of bacterial genera in advanced AMD patients and the significant differences in key microbiota-associated SCFA and BA metabolites between cohorts—especially among intermediate and advanced groups—add further support to links between gut dysbiosis and AMD progression. However, it is essential to note that increased diversity alone does not universally indicate pathology; rather, its implications vary depending on microbial taxa involved and the host's context, particularly in immune-mediated diseases such as AMD.

In addition, we acknowledge that the small sample size and group heterogeneity in terms of sex, race, and AMD subtype may have contributed to the variability in the observed taxonomic composition. Although some of the observed differences in bacterial abundances were influenced by patients with more severe AMD, the significant findings predominantly arise from this subset, highlighting an essential characteristic of our AMD cohort. Despite these limitations, we believe the data presented here accurately

Investigative Ophthalmology & Visual Science

reflect preliminary insights into potential AMD-specific gut microbial alterations, warranting further investigation.

Continued research with broader patient populations and longitudinal follow-up may help to validate these findings, develop new strategies for discovery of novel biomarkers of risk for AMD progression, and explore potential therapeutic interventions targeting the gut microbiome to influence AMD outcomes. Integrating functional and clinical data in future studies will be crucial to determine whether observed microbiome changes correspond to true dysbiosis or adaptive alterations in response to AMD pathology. Future validation in larger, more diverse cohorts will also be critical to confirm these observations and reduce the potential influence of outliers, ensuring robust and reproducible findings.

Acknowledgments

Supported by the FORE-I Foundation (DS); a grant from the BrightFocus Foundation (M2018042 to DS); Illinois Society for the Prevention of Blindness; The University of Chicago Women's Board (DS); Institute for Translational Medicine (DS); a grant from the National Institute of Diabetes and Digestive and Kidney Diseases, National Institutes of Health (P30 DK42086 to EBC); and a Thome Memorial Foundation award grant (DS).

Disclosure: **Z. Parekh**, None; **J. Xiao**, None; **A. Mani**, None; **Q. Evans**, None; **C. Phung**, None; **H.A. Barba**, None; **B. Xie**, None; **A.M. Sidebottom**, None; **A. Sundararajan**, None; **H. Lin**, None; **R. Ramaswamy**, None; **D. Dao**, None; **R. Gonnah**, None; **M. Yehia**, None; **S.M. Hariprasad**, None; **M. D'Souza**, None; **D. Sulakhe**, None; **E.B. Chang**, None; **D. Skondra**, None

References

1. Rein DB, Wittenborn JS, Burke-Conte Z, et al. Prevalence of age-related macular degeneration in the US in 2019. *JAMA Ophthalmol*. 2022;140:1202–1208.
2. Mousavi M, Armstrong RA. Genetic risk factors and age-related macular degeneration (AMD). *J Optom*. 2013;6:176–184.
3. Gehrs KM, Anderson DH, Johnson LV, Hageman GS. Age-related macular degeneration—emerging pathogenetic and therapeutic concepts. *Ann Med*. 2006;38:450–471.
4. Bressler SB. Introduction: understanding the role of angiogenesis and antiangiogenic agents in age-related macular degeneration. *Ophthalmology*. 2009;116:S1–S7.
5. Lim LS, Mitchell P, Seddon JM, Holz FG, Wong TY. Age-related macular degeneration. *Lancet*. 2012;379:1728–1738.
6. Seddon JM. Dietary fat and risk for advanced age-related macular degeneration. *Arch Ophthalmol*. 2001;119:1191.
7. Skondra D. Effects of ApoE deficiency, aging and high fat diet on laser-induced choroidal neovascularization and Bruch's membrane–RPE interface morphology. *Invest Ophthalmol Vis Sci*. 2007;48:1768–1768.
8. Seddon JM, Cote J, Rosner B. Progression of age-related macular degeneration. *Arch Ophthalmol*. 2003;121:1728–1737.
9. Nunes S, Alves D, Barreto P, et al. Adherence to a Mediterranean diet and its association with age-related macular degeneration. The Coimbra Eye Study-Report 4. *Nutrition*. 2018;51–52:6–12.
10. Lin P, McClintic SM, Nadeem U, Skondra D. A review of the role of the intestinal microbiota in age-related macular degeneration. *J Clin Med*. 2021;10:2072.
11. Xiao J, Xie B, Dao D, et al. High-fat diet alters the retinal pigment epithelium and choroidal transcriptome in the absence of gut microbiota. *Cells*. 2022;11:2076.
12. Zhang JY, Xie B, Barba H, et al. Absence of gut microbiota is associated with RPE/choroid transcriptomic changes related to age-related macular degeneration pathobiology and decreased choroidal neovascularization. *Int J Mol Sci*. 2022;23:9676.
13. Rowan S, Jiang S, Korem T, et al. Involvement of a gut–retina axis in protection against dietary glycemia-induced age-related macular degeneration. *Proc Natl Acad Sci USA*. 2017;114:E4472–E4481.
14. Zinkernagel MS, Zysset-Burri DC, Keller I, et al. Association of the intestinal microbiome with the development of neovascular age-related macular degeneration. *Sci Rep*. 2017;7:40826.
15. Al Bander Z, Nitert MD, Mousa A, Naderpoor N. The gut microbiota and inflammation: an overview. *Int J Environ Res Public Health*. 2020;17:7618.
16. Nadeem U, Xie B, Movahedan A, et al. High throughput RNA sequencing of mice retina reveals metabolic pathways involved in the gut–retina axis. *bioRxiv*. 2020, https://doi.org/10.1101/2020.10.01.318949.
17. Zysset-Burri DC, Keller I, Berger LE, et al. Associations of the intestinal microbiome with the complement system in neovascular age-related macular degeneration. *NPJ Genom Med*. 2020;5:34.
18. Xiao J, Zhang JY, Luo W, He PC, Skondra D. The emerging role of gut microbiota in age-related macular degeneration. *Am J Pathol*. 2023;193:1627–1637.
19. Zwielehner J, Lassl C, Hippe B, et al. Changes in human fecal microbiota due to chemotherapy analyzed by TaqMan-PCR, 454 sequencing and PCR-DGGE fingerprinting. *PLoS One*. 2011;6:e28654.
20. Zheng J, Sun Q, Zhang J, Ng SC. The role of gut microbiome in inflammatory bowel disease diagnosis and prognosis. *United European Gastroenterol J*. 2022;10:1091–1102.
21. Lin X-H, Jiang J-K, Luo J-C, et al. The long term microbiota and metabolic status in patients with colorectal cancer after curative colon surgery. *PLoS One*. 2019;14:e0218436.
22. Flaxel CJ. Age-related macular degeneration Preferred Practice Pattern. *Ophthalmology*. 2020;127:1–65.
23. Chew EY, Clemons T, SanGiovanni JP, et al. The Age-Related Eye Disease Study 2 (AREDS2): study design and baseline characteristics (AREDS2 report number 1). *Ophthalmology*. 2012;119:2282–2289.
24. Danis RP, Domalpally A, Chew EY, et al. Methods and reproducibility of grading optimized digital color fundus photographs in the Age-Related Eye Disease Study 2 (AREDS2 report number 2). *Invest Ophthalmol Vis Sci*. 2013;54:4548–4554.
25. Ho JTK, Chan GCF, Li JCB. Systemic effects of gut microbiota and its relationship with disease and modulation. *BMC Immunol*. 2015;16:21.
26. Yu Y, Reynolds R, Rosner B, Daly MJ, Seddon JM. Prospective assessment of genetic effects on progression to different stages of age-related macular degeneration using multistate Markov models. *Invest Ophthalmol Vis Sci*. 2012;53:1548–1556.
27. Awh CC, Hawken S, Zanke BW. Treatment response to antioxidants and zinc based on CFH and ARMS2 genetic risk allele number in the Age-Related Eye Disease Study. *Ophthalmology*. 2015;122:162–169.
28. Bolger AM, Lohse M, Usadel B. Trimmomatic: a flexible trimmer for Illumina sequence data. *Bioinformatics*. 2014;30:2114–2120.
29. Wood DE, Lu J, Langmead B. Improved metagenomic analysis with Kraken 2. *Genome Biol*. 2019;20:257.
30. Lu J, Breitwieser FP, Thielen P, Salzberg SL. Bracken: estimating species abundance in metagenomics data. *PeerJ Comput Sci*. 2017;3:e104.

31. Blanco-Míguez A, Beghini F, Cumbo F, et al. Extending and improving metagenomic taxonomic profiling with uncharacterized species using MetaPhlAn 4. *Nat Biotechnol*. 2023;41:1633–1644.
32. Beghini F, McIver LJ, Blanco-Míguez A, et al. Integrating taxonomic, functional, and strain-level profiling of diverse microbial communities with bioBakery 3. *eLife*. 2021;10:e65088.
33. Wickham H, Averick M, Bryan J, et al. Welcome to the tidyverse. *J Open Source Softw*. 2019;4:1686.
34. Haak BW, Littmann ER, Chaubard J-L, et al. Impact of gut colonization with butyrate-producing microbiota on respiratory viral infection following allo-HCT. *Blood*. 2018;131:2978–2986.
35. Stutz MR, Dylla NP, Pearson SD, et al. Immunomodulatory fecal metabolites are associated with mortality in COVID-19 patients with respiratory failure. *Nat Commun*. 2022;13:6615.
36. den Hollander AI, de Jong EK. Highly penetrant alleles in age-related macular degeneration. *Cold Spring Harb Perspect Med*. 2015;5:a017202.
37. Yates JRW, Sepp T, Matharu BK, et al. Complement C3 variant and the risk of age-related macular degeneration. *N Engl J Med*. 2007;357:553–561.
38. McMurdie PJ, Holmes S. phyloseq: an R package for reproducible interactive analysis and graphics of microbiome census data. *PLoS One*. 2013;8:e61217.
39. Fernandes AD, Reid JN, Macklaim JM, McMurrough TA, Edgell DR, Gloor GB. Unifying the analysis of high-throughput sequencing datasets: characterizing RNA-seq, 16S rRNA gene sequencing and selective growth experiments by compositional data analysis. *Microbiome*. 2014;2:15.
40. Robinson MD, McCarthy DJ, Smyth GK. edgeR: a Bioconductor package for differential expression analysis of digital gene expression data. *Bioinformatics*. 2010;26:139–140.
41. Ackerman HD, Gerhard GS. Bile acids in neurodegenerative disorders. *Front Aging Neurosci*. 2016;8:263.
42. Salem F, Kindt N, Marchesi JR, et al. Gut microbiome in chronic rheumatic and inflammatory bowel diseases: similarities and differences. *United European Gastroenterol J*. 2019;7:1008–1032.
43. Devkota S, Wang Y, Musch MW, et al. Dietary-fat-induced taurocholic acid promotes pathobiont expansion and colitis in Il10−/− mice. *Nature*. 2012;487:104–108.
44. David LA, Maurice CF, Carmody RN, et al. Diet rapidly and reproducibly alters the human gut microbiome. *Nature*. 2014;505:559–563.
45. Murros KE, Huynh VA, Takala TM, Saris PEJ. *Desulfovibrio* bacteria are associated with Parkinson's disease. *Front Cell Infect Microbiol*. 2021;11:652617.
46. Bai J, Wan Z, Zhang Y, Wang T, Xue Y, Peng Q. Composition and diversity of gut microbiota in diabetic retinopathy. *Front Microbiol*. 2022;13:926926.
47. Huang Y, Wang Z, Ma H, et al. Dysbiosis and implication of the gut microbiota in diabetic retinopathy. *Front Cell Infect Microbiol*. 2021;11:646348.
48. Singh SB, Carroll-Portillo A, Lin HC. *Desulfovibrio* in the gut: the enemy within? *Microorganisms*. 2023;11:1772.
49. Renson A, Harris KM, Dowd JB, et al. Early signs of gut microbiome aging: biomarkers of inflammation, metabolism, and macromolecular damage in young adulthood. *J Gerontol A Biol Sci Med Sci*. 2020;75:1258–1266.
50. Wang Q, Zhang S-X, Chang M-J, et al. Characteristics of the gut microbiome and its relationship with peripheral CD4+ T cell subpopulations and cytokines in rheumatoid arthritis. *Front Microbiol*. 2022;13:799602.
51. Heddes M, Altaha B, Niu Y, et al. The intestinal clock drives the microbiome to maintain gastrointestinal homeostasis. *Nat Commun*. 2022;13:6068.
52. Turnbaugh PJ, Ley RE, Hamady M, Fraser-Liggett CM, Knight R, Gordon JI. The human microbiome project. *Nature*. 2007;449:804–810.
53. Gutierrez Lopez DE, Lashinger LM, Weinstock GM, Bray MS. Circadian rhythms and the gut microbiome synchronize the host's metabolic response to diet. *Cell Metabolism*. 2021;33:873–887.
54. Liu Z, Wei Z-Y, Chen J, et al. Acute sleep–wake cycle shift results in community alteration of human gut microbiome. *mSphere*. 2020;5:e00914–e00919.
55. Klein RJ, Zeiss C, Chew EY, et al. Complement factor H polymorphism in age-related macular degeneration. *Science*. 2005;308:385–389.
56. Sardell RJ, Persad PJ, Pan SS, et al. Progression rate from intermediate to advanced age-related macular degeneration is correlated with the number of risk alleles at the CFH locus. *Invest Ophthalmol Vis Sci*. 2016;57:6107–6115.
57. Gold B, Merriam JE, Zernant J, et al. Variation in factor B (*BF*) and complement component 2 (*C2*) genes is associated with age-related macular degeneration. *Nat Genet*. 2006;38:458–462.
58. Maller JB, Fagerness JA, Reynolds RC, Neale BM, Daly MJ, Seddon JM. Variation in complement factor 3 is associated with risk of age-related macular degeneration. *Nat Genet*. 2007;39:1200–1201.
59. Dietzel M, Pauleikhoff D, Arning A, et al. The contribution of genetic factors to phenotype and progression of drusen in early age-related macular degeneration. *Graefes Arch Clin Exp Ophthalmol*. 2014;252:1273–1281.
60. Hou X-W, Wang Y, Pan C-W. Metabolomics in age-related macular degeneration: a systematic review. *Invest Ophthalmol Vis Sci*. 2020;61:13.
61. Brown CN, Green BD, Thompson RB, den Hollander AI, Lengyel I. Metabolomics and age-related macular degeneration. *Metabolites*. 2018;9:4.
62. den Besten G, van Eunen K, Groen AK, Venema K, Reijngoud D-J, Bakker BM. The role of short-chain fatty acids in the interplay between diet, gut microbiota, and host energy metabolism. *J Lipid Res*. 2013;54:2325–2340.
63. Erny D, Dokalis N, Mezö C, et al. Microbiota-derived acetate enables the metabolic fitness of the brain innate immune system during health and disease. *Cell Metab*. 2021;33:2260–2276.e7.
64. Silva YP, Bernardi A, Frozza RL. The role of short-chain fatty acids from gut microbiota in gut-brain communication. *Front Endocrinol (Lausanne)*. 2020;11:25.
65. Horai R, Zárate-Bladés CR, Dillenburg-Pilla P, et al. Microbiota-dependent activation of an autoreactive T cell receptor provokes autoimmunity in an immunologically privileged site. *Immunity*. 2015;43:343–353.
66. Nakamura YK, Janowitz C, Matea C, et al. Short chain fatty acids ameliorate immune-mediated uveitis partially by altering migration of lymphocytes from the intestine. *Sci Rep*. 2017;7:11745.
67. Lyzogubov V, Dasso M, Bora N, Bora PS. Role of thalidomide, senicapoc, and sodium butyrate in choroidal neovascularization. *Biochem Biophys Res Commun*. 2020;530:367–373.
68. Xiao X, Chen M, Xu Y, et al. Sodium butyrate inhibits neovascularization partially via TNXIP/VEGFR2 pathway. *Oxid Med Cell Longev*. 2020;2020:e6415671.
69. Dos Reis JS, Dos Reis Teixeira A, De Vasconcelos Quaresma A, et al. Sodium butyrate-loaded nanoparticles coated with chitosan for the treatment of neovascularization in age-related macular degeneration: ocular biocompatibil-

Investigative Ophthalmology & Visual Science

ity and antiangiogenic activity. *Eur J Pharm Biopharm*. 2022;179:26–36.
70. Warden C, Barnett JM, Brantley MA. Taurocholic acid inhibits features of age-related macular degeneration in vitro. *Exp Eye Res*. 2020;193:107974.
71. Xu N, Bai Y, Han X, et al. Taurochenodeoxycholic acid reduces astrocytic neuroinflammation and alleviates experimental autoimmune encephalomyelitis in mice. *Immunobiology*. 2023;228:152388.
72. Xue R, Su L, Lai S, et al. Bile acid receptors and the gut–liver axis in nonalcoholic fatty liver disease. *Cells*. 2021;10:2806.
73. Ochiai T, Nagayama T, Matsui K, et al. Tauroursodeoxycholic acid attenuates diet-induced and age-related peripheral endoplasmic reticulum stress and cerebral amyloid pathology in a mouse model of Alzheimer's disease. *J Prev Alzheimers Dis*. 2021;8:483–494.
74. Wang C-F, Yuan J-R, Qin D, et al. Protection of tauroursodeoxycholic acid on high glucose-induced human retinal microvascular endothelial cells dysfunction and streptozotocin-induced diabetic retinopathy rats. *J Ethnopharmacol*. 2016;185:162–170.
75. Tao Y, Dong X, Lu X, et al. Subcutaneous delivery of tauroursodeoxycholic acid rescues the cone photoreceptors in degenerative retina: a promising therapeutic molecule for retinopathy. *Biomed Pharmacother*. 2019;117:109021.
76. Lawson EC, Bhatia SK, Han MK, et al. Tauroursodeoxycholic acid protects retinal function and structure in rd1 mice. *Adv Exp Med Biol*. 2016;854:431–436.
77. Kiang L, McClintic S, Saleh M, et al. The gut microbiome in advanced age-related macular degeneration. *Invest Ophthalmol Vis Sci*. 2017;58:5739.
78. Osborn MP, Park Y, Parks MB, et al. Metabolome-wide association study of neovascular age-related macular degeneration. *PLoS One*. 2013;8:e72737.
79. Husain A, Sato D, Jeelani G, Soga T, Nozaki T. Dramatic increase in glycerol biosynthesis upon oxidative stress in the anaerobic protozoan parasite *Entamoeba histolytica*. *PLoS Negl Trop Dis*. 2012;6:e1831.
80. Diacovich L, Lorenzi L, Tomassetti M, Méresse S, Gramajo H. The infectious intracellular lifestyle of *Salmonella enterica* relies on the adaptation to nutritional conditions within the *Salmonella*-containing vacuole. *Virulence*. 2017;8:975–992.
81. Kador PF, Takahashi Y, Akagi Y, Blessing K, Randazzo J, Wyman M. Age-dependent retinal capillary pericyte degeneration in galactose-fed dogs. *J Ocul Pharmacol Ther*. 2007;23:63–69.
82. Kinoshita JH, Fukushi S, Kador P, Merola LO. Aldose reductase in diabetic complications of the eye. *Metabolism*. 1979;28:462–469.
83. Kern TS, Engerman RL. Microvascular metabolism in diabetes. *Metabolism*. 1986;35:24–27.
84. Stambolian D. Galactose and cataract. *Surv Ophthalmol*. 1988;32:333–349.
85. Morohoshi K, Goodwin AM, Ohbayashi M, Ono SJ. Autoimmunity in retinal degeneration: autoimmune retinopathy and age-related macular degeneration. *J Autoimmun*. 2009;33:247–254.
86. Richard DM, Dawes MA, Mathias CW, et al. L-Tryptophan: basic metabolic functions, behavioral research and therapeutic indications. *Int J Tryptophan Res*. 2009;2:45–60.
87. Sorgdrager FJH, Naudé PJW, Kema IP, Nollen EA, Deyn PPD. Tryptophan metabolism in inflammaging: from biomarker to therapeutic target. *Front Immunol*. 2019;10:2565.

Investigative Ophthalmology & Visual Science